A new approach for defect detection in X-ray CT images

Abstract. We introduce a novel method to automatically evaluate X-ray computed tomography (CT) images for the purpose of detecting material defects by evaluating the significance of features extracted by first order derivative filters. We determine the noise characteristics of an image using robust estimation methods and compute the noise of the filtered image via error propagation. The significance of these features can then be evaluated based on the signal-to-noise ratio in the filtered image. The major benefit of that procedure is, that a sample-independent threshold on the signal-to-noise ratio can be chosen. The results are demonstrated on parts drawn from an industrial manufacturing line.

1 Introduction

X-ray computed tomography (CT) enjoys a growing interest in industrial quality control as it can be used on a wide range of products and provides detailed information about otherwise unaccessible features. Major application areas are the inspection of castings, the detection of gas bubbles or inclusions and cracks. Image processing algorithms should be robust to cope with the noise and poor contrast characteristic of X-ray images.

1.1 Review of related work

An overview of methods for flaw detection in castings is given in [1]. In early methods, the image data are compared to data obtained from a reference object. This approach requires either exact repositioning of the probes or a matching of the image data, which is non-trivial and computationally expensive. Also, these methods cannot allow for tolerances in the manufacturing process. In the case of castings it is not even possible to produce a reference part that is totally free of defects. Here, the question is rather whether or not these defects are critical. An alternative strategy is to generate a reference object from the image data themselves. Several such methods have been proposed, most of which are based on modifications of median filtering techniques [2,3,4,5,6]. They basically differ in the way the filter masks are adapted to the structure of the object and the choice of threshold value for fault detection. However, these methods have difficulty in detecting small low-contrast defects such as cracks. Also, the threshold values are chosen either empirically or based on rarely justified assumptions such as two-mode histograms.

In another approach, local areas are analyzed for defects based on their Fourier transform [7]. This technique, however, does not distinguish between defects and noise. Multi-resolution image analysis [8] has similar drawbacks, i.e. poor performance on low-contrast noisy images.

This paper suggests a solution to both, the challenge to detect coherent structures in noisy images, and the issue of systematically choosing the proper threshold for detection.

2 Modeling and descriptive statistics of the image

We model the absorption $g(x)$ of an intact object as locally homogeneous with added correlated isotropic normal noise. In other words, we interpret the data as realization of a stochastic process with drift (the mean is only locally constant). The covariance structure is assumed constant throughout the random field (homoscedasticity), and it is estimated based on a homogeneous training region (see fig. 2a). The probability of a voxel being intact can then be estimated using statistical tests at a chosen significance level. If a moderate significance level is chosen to reduce errors of the second kind[1], a large number of pseudo errors result — at a significance level of 95%, for instance, $(1 - 0.95) \cdot 10^3 = 50$ pixels will be marked as defect in an intact cube with a length of 10 pixels. We therefore need to apply techniques that smooth out the noise and enhance the defects (section 3). If we still wish to calculate probabilities, we need to see what happens to the noise under the filtering operations, see section 4.

3 Defect Enhancement

The key to defect enhancement is to detect oriented structures within the image. Commonly used techniques are tensorial approaches, which are discussed in [9,10,11,12]. These methods require eigenvalue computation for each pixel, which results in a computationally expensive procedure. In addition they yield equal responses to edges and to noise. As an alternative, we suggest to simply take the square of locally averaged derivates as an edge detector.This suppresses the noise and - add the same time - enhances pixels within areas of coherent grey value structure. The corresponding operator looks like this:

$$F\left\{g(\boldsymbol{x})\right\} = \sum_{p=1}^{3} \left(\int w(\boldsymbol{x} - \boldsymbol{x'}) \frac{\partial g(\boldsymbol{x'})}{\partial x_p} d\boldsymbol{x'} \right)^2 \tag{1}$$

where p runs over the spatial directions. Fig. 1 shows the result obtained on an artificial image with a defect simulated as a vertical crack in the center. The crack appears as a signal in front of the noisy background. The transformations can be implemented discretely by applying x-,y- and z-derivative and smoothing filters to the image $g(x)$ and summing the square of these terms.

---

[1] In this context, an error of the second kind means classifying a defect voxel as intact.
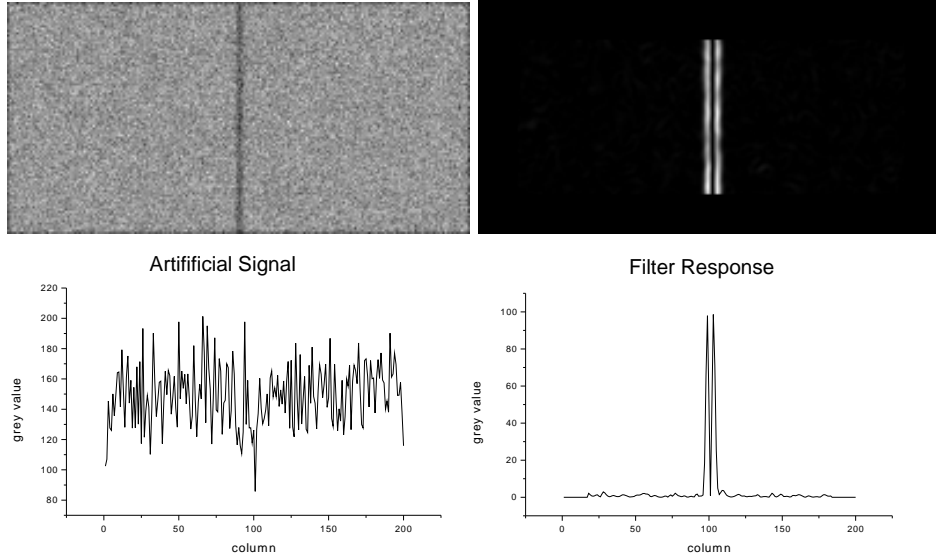
Fig. 1: Artificial test image. Upper left: XY cross section through artificial volume data with a planar crack parallel to the YZ plane. We added uncorrelated normal noise (with standard deviation $\sigma = 20$) to the image and finally convolved it with a binomial mask of size 5 to obtain correlated noise. Upper right: Test image after filtering according to (1). Lower left: horizontal cross section through the upper left image displayed as a signal. Lower right: horizontal cross section through the processed image.

4   Error propagation

This section details how the transformation in (1) affects the noise. Differentiation and smoothing are performed by a single filter f. This can be expressed as

$$g'_{(i,j,k)} = \sum_{\{l,m,n\}=-r}^{r} f_{(l,m,n)} g_{(i-l,j-m,k-n)} \tag{2}$$

If the image is modeled as a random field as described in section 2, the variance of $g'_{(i,j,k)}$ is

$$\sigma^2_{(i,j,k)} = E\left[\left(g'_{(i,j,k)} - E\left[g'_{(i,j,k)}\right]\right)^2\right], \tag{3}$$

where E denotes expectation. We substitute (2) into (3), rearrange terms and compute the expectation value term by term in order to obtain

$$\sigma^2_{(i,j,k)} = \sum_{\{l,m,n,o,p,q\}=-r}^{r} f_{(l,m,n)} f_{(o,p,q)}$$
$$E\left[\left(g_{(i-l,j-m,k-n)} - E\left[g_{(i-l,j-m,k-n)}\right]\right)\left(g_{(i-o,j-p,k-q)} - E\left[g_{(i-o,j-p,k-q)}\right]\right)\right] \tag{4}$$

Eq. 4 can be rewritten as

$$\sigma^2_{(i,j,k)} = \sum_{\{l,m,n,o,p,q\}=-r}^{r} f_{(l,m,n)} f_{(o,p,q)} Cov(i-l,j-m,k-n,i-o,j-p,k-q). \tag{5}$$

As mentioned above, we assume the covariance function to be constant over space so that the variance at a pixel becomes

$$\sigma^2 = \sum_{\{l,m,n,o,p,q=-r\}}^{r} f_{(l,m,n)} f_{(o,p,q)} Cov(l-o,n-p,n-q). \tag{6}$$

The value of σ^2 is determined based on a training region as shown in Fig. 2a. The size of that region has to be at least 2 times the filter size in each direction, so that all covariances in (6) can be accounted for. It might be larger for the benefit of statistically more precise results at the cost of execution time. The average grey value used in the covariance matrix corresponds to the arithmetic mean within the training region. Fig. 2 illustrates that it is indeed necessary to include the off-diagonal terms of the covariance function in (6): The noise is highly correlated.

To compute the square of the random variables in (1) consider a Gaussian random variable y with zero mean and variance σ_y^2. The variance of y^2 is by definition

$$\sigma_{y^2}^2 = E[y^4] - E[y^2]^2 \tag{7}$$

and

$$E[y^2]^2 = \sigma_y^4 \tag{8}$$

$$E[y^4] = 3\sigma_y^4 \tag{9}$$

Substituting (8) and (9) in (7) yields

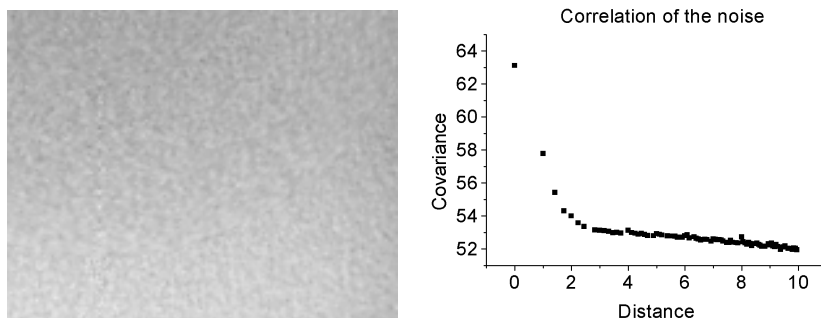$$\sigma_{y^2}^2 = 2\sigma_y^4 \tag{10}$$

Fig. 2: Analyzing the correlation of the noise in real data. Left: Homogenous region within a real object; right: Autocovariance vs. distance for the image to the left. The noise within that region is highly correlated, as can be seen from the slowly decaying autocovariance function (note the scale on the vertical axis).

The last step of (1) consists in taking the sum of random variables. Even though the derivatives of a random field are spatially correlated, the derivatives with respect to different spatial directions taken at the *same* point are *un*correlated in an isotropic random field. Assuming isotropy, the variance of the sum in (1) is equal to the sum of the individual variances. Using that and equations (6) and (10) we note that the variance σ_F^2 of the filtered image becomes

$$\sigma_F^2 = 6\sigma^4 \tag{11}$$

where σ^2 is given by (6). We finally compute the signal-to-noise ratio:

$$SNR_F = \frac{F\{g(\boldsymbol{x})\}}{\sigma_F} \tag{12}$$

There is one drawback of this operator with respect to the purpose of detecting cracks: Since it yields the strongest response in areas where there is a predominating gradient direction across a local neighborhood, it will yield a stronger response to edges than to cracks. We attempted to work around this problem by subtracting the original image from the image obtained after a closing operation. While defects disappear after the closing, edges should remain relatively unchanged. This worked on some data, but did not prove to be a reliable method in general. At this point, therefore, we merely have to exclude regions close to the object boundary from consideration. In other words: We can so far only detect defects in the interior of the object and label the remaining part of the image as invalid. To determine the valid region we choose a global threshold, which we determine dynamically from the histogram as described in the following section.
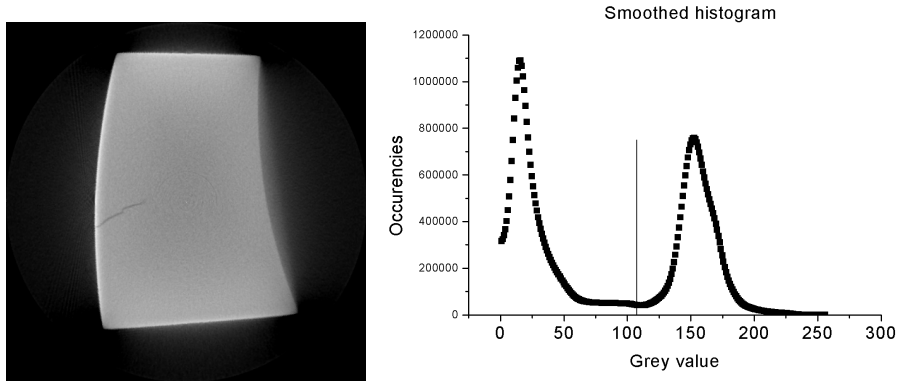
Fig. 3: Approximate segmentation of the data. Left: Cross section through a CT-image of a massive steel part with a crack, that has to be detected; right: Typical histogram of a one-component object after smoothing. The threshold value is placed at the minimum between the two peaks

5 Excluding the boundary region

Fig. 3 shows a histogram typical for one-component CT-images with strong X-ray absorption: It actually contains two major peaks, the right one of coming from the material itself and the other one arising due to artefacts in the outer region close to the object. Based on this grey value distribution, we perform an approximate segmentation by choosing the minimum between the two major peaks as a threshold. To ensure the uniqueness of this minimum, we apply an iterative smoothing algorithm to the histogram, which works as follows: Smooth the histogram with a (3×1) binomial mask, count the total number of maxima and repeat this procedure until we're left with exactly two maxima. This strategy allows an approximate distinction between object and background for one- as well as for multiple-component images. We then define the interior region of the object by eroding the binarized image. Defect detection will only be meaningful within the thus obtained region.

6 Experimental Results

Fig. 4 summarizes the defect detection algorithm and quantifies the parameters used. We apply the operator described by (12) to the original image and detect defects by applying a threshold on the region of interest, that excludes areas close to the object boundaries. The left picture of Fig. 5 shows the original image
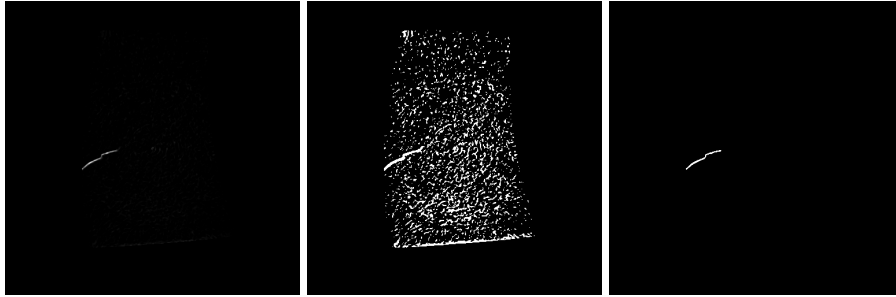
Fig. 5: Left: Data set shown in fig. 3 after filtering with f. 3D Image size: $511 \times 511 \times 280$ pixels; center: the left image binarized at a threshold of 1; right binarization at 13.

processed according to (12). The center and right figures show the processed image binarized at a threshold value of 1 and 13 respectively. The filter f is generated by convolving a $(5 \times 5 \times 5)$ Gaussian with the $(3 \times 3 \times 3\times)$ derivative operator [13], that has been optimized for isotropy. The image is filtered accordingly, whereby we took advantage of filter separability, of course. The other parameters are the number of components - one in the example - and the size of the mask used for eroding the region that has been determined to be the object region after the histogram-based thresholding explained in the previous section. For faster processing it is desirable to process the image at a lower-than-original resolution as the feature size permits. In the example the crack could still be detected savely at half the original resolution.
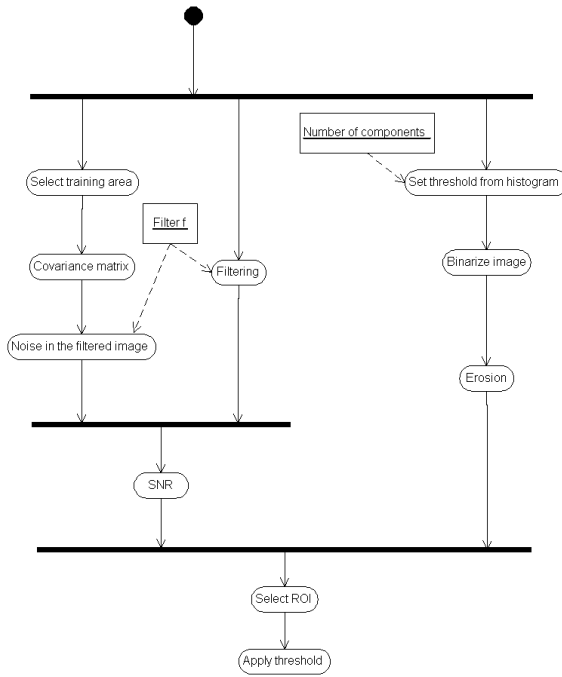

Fig. 4: Schematic summary of the image processing procedure. Parameters: f: $(5 \times 5 \times 5)$ Gaussian convolved with $(3 \times 3 \times 3)$ derivative operator; number of components: 1; mask size used for erosion: (5×1) applied in each direction.

7   Conclusion

We proposed a rather general method to detect defects in CT-images as structural deviations from the local background. We demonstrated its effectiveness on cracks, which are difficult to detect with other methods. Other than earlier publications, we used linear filters together with neighborhoud information to emphasize the defects, and - in addition - outlined a mechanism that allows for a rather systematic than heuristic choice of the detection threshold. We intend to apply the framework to other types of faults by adapting the linear filter used for defect enhancement.

References

1. D. Mery et. al. Automated quality control of castings: state of the art (German). *Technisches Messen*, 68, 2001.
2. D. Filbert et al. Computer aided inspection of castings. In *IEEE-IAS Annual Meeting*, pages 1087–1095, 1987.
3. W. Heinrich. A speed optimized rank ordering operator for the automation of the radiological inspection of castings. Technical Report 123, Institute for Electrical Engineering, Technical University of Berlin, 1987.
4. W.Heinrich. *Automated X-ray inspection of castings in series*. PhD thesis, Institute for Electrical Engineering, Technical University of Berlin, 1988.
5. H. Hecker und D. Filbert. X-ray inspection: Automatic adaption of an inspection system to inspection tasks (in German). In *DGZfP Annual Meeting*, volume 33.2, pages 655–660, 1992.
6. H. Hecker. *A new method for the evaluation of X-ray images for the automated inspection of castings (In German)*. PhD thesis, Institute for Electrical Engineering, Technical University of Berlin, 1995.
7. A. Gayer et al. Automatic recognition of welding defects in real-time radiography. *NDT International*, 23(4):131–136, 1990.
8. Y. Chitti. Detection of small intensity changes in CCD images with non-uniform illumination and large signal dependent noise. *CVGIP: Graph. Models and Image Processing*, 59(3):139–148, 1997.
9. J. Bigün and G.H. Granlund. Optimal detection of linear symmetry. In *Proceedings ICCV'87, London 1987*, pages 433–438, Washington,DC, 1987. IEEE, IEEE Computer Society Press.
10. H. Knutsson. Representing local structure using tensors. In *The 6th Scandinavian Conference on Image Analysis*, Oulu, Finland, June 19-22 1989.
11. A.R. Rao and B.G. Schunk. Computing oriented texture fields. In *Proceedings CVPR'89, San Diego, CA*, pages 61–68, Washington, DC, 1989. IEEE, IEEE Computer Society Press.
12. A.R. Rao. *A taxonomy for texture description and identification*. Springer, New York, 1990.
13. H. Scharr. *Optimal operators in Digital Image Processing*. PhD thesis, University of Heidelberg, 2000.